17th World Conference on Earthquake Engineering, 17WCEE
Sendai, Japan - September 13th to 18th 2020

LATERAL LOAD PERFORMANCE EVALUATION OF UNBONDED STRIP-STRP BASE ISOLATOR

M. B. Zisan[(1)], A. Igarashi[(2)]

[(1)] *Ph.D. Candidate, Dept. Urban Management, Kyoto University, Kyoto 611-0011, Japan, email: zisan.basir.33m@st.kyoto-u.ac.jp*
[(2)] *Professor, DPRI, Kyoto University, Kyoto 611-0011, Japan, email: igarashi.akira.7m@kyoto-u.ac.jp*

Abstract

The Scrap Tire Rubber Pad (STRP) made by natural or synthetic rubber and high strength reinforcing cords exhibits substantial vertical stiffness and horizontal flexibility, and this property can be regarded as ideal for seismic isolators for structures. The use of environmentally burdensome scrape tires as STRP might be convenient as an efficient and low-cost solution for the implementation of aseismic design philosophy for low-to-medium rise buildings, especially in developing countries. Finite Element (FE) analysis of an unbonded strip-STRP isolator, subjected to a combination of gravity load and lateral loads is conducted to investigate its lateral load performance. The rubber of the isolator is modelled with Mooney-Rivlin hyperelastic and Proney viscoelastic materials including the Mullins material damage effect. Model verification and response evaluation are carried out for cyclic loads acting along two orthogonal lateral directions. The influence of the length-to-width ratio to the isolator performance in terms of the force-displacement relationships, horizontal stiffness, structural damping and isolation periods is evaluated. Stable rollover deformation causes stiffening behavior at greater deformation levels followed by a significant stiffness reduction in the intermediate lateral strain range. These properties can provide an advantage to the use of STRP in seismic isolation effectiveness for the design-basis earthquake and limiting the bearing displacement under MCE level earthquakes. The efficacy of the isolators at different levels of seismic hazards is verified with ASCE/SEI 7-2010 seismic provision. Findings of the FE analysis provide a preliminary design basis of strip-STRP isolators.

Keywords: Lateral load, Strip-STRP isolator, Unbonded application, DBE & MCE, FEM.

1 Introduction

In order to implement the seismic isolation technique to structures, several types of seismic isolators are used in structural design and construction practice. Although the steel reinforced elastomeric isolator (SREI) is the most popular, the disadvantage of SREI in the production cost due to labor-intensive manufacturing and vulcanization processes [1] makes its application limited to large, expensive and sophisticated structures [2, 3]. Besides, 'overly burdensome requirements' for design certification is a barrier to the adaption of the SREI system [3]. To extend the earthquake-resistant design strategy for masonry and historical structures, public buildings including school, hospital and residential structures, etc., the cost reduction and simplicity of the design principle are of great concern. As alternatives, several aseismic tools made of locally available inexpensive and light-weight materials have been proposed [4~8]. The fiber-reinforced elastomeric isolator (FREI) in which fiber reinforcement is used instead of steel shims [9] is considered to be lightweight and cost-effective. FREI not only exhibits superior performance and higher damping [10~15] but also can be fabricated with any size from a long rectangular strip. Also, FREI shows better performance without any mechanical fastening that eschews the usage of large endplates in SREI [14, 16~18]. Scrap tires are made by vulcanization of natural or synthetic rubber with interleaved reinforcing cords. This material is regarded as cheap and environmentally friendly for isolation of low to medium-rise buildings [6, 19, 20]. The scrape tire rubber pad (STRP) has an equivalent damping ratio of approximately 10~22% and a vertical to horizontal stiffness ratio exceeding 150 [21~23]. Those properties of the scrape tire pad satisfy the requirement as a suitable isolation material [24, 25]. For structures made of masonry or concrete walls, the strip shape isolator is expected to be

a cost-effective component of seismic isolation application since a strong base foundation is not required [1, 9, 26] as opposed to the application of SREI. Although a strip shape isolator is more suitable to those types of structures, the previous studies on the scrape tire isolator is limited to the types of slender shapes with an aspect ratio of 2.08, and such devices are considered to be unstable at lower strain levels [18]. For this reason, this study focuses on strip shape STRP isolators with limited height. The lateral load performance of strip STRP isolators under two orthogonal loading conditions is investigated by means of FE analysis.

2 Scrape Tire Rubber Pad (STRP) Isolator

Vehicle tires are made by vulcanization of rubber material and embedded reinforcing cords. These cords are placed in the form of a layer and orientated in some specific directions. The preparation procedure of a 12mm thick STRP layer from a typical radial tire is shown in Fig. 1 [21]. STRP made from Bridgestone 385/65R22.5 tyre typically has five reinforcement layers oriented by ±70° with respect to carcass steel, as shown in Fig. 2. An STRP isolator is made by stacking individual STRP layers one above another and then bonded by adhesive. The geometric properties of strip-STRP isolators considered for the current study is shown in Table 1. Each isolator consists of two STRP layers with a fixed height and width of 24 mm and 72 mm, respectively. The equivalent thickness of elastomer and that of the reinforcement layers are assumed to be 2.4 mm and 0.4 mm, respectively. Shape factors of the isolator are varied from 7.5 to 13.6 and length-width ratios (l/w) along the longitudinal direction (R_l) are changed from 3.0 to 30. To satisfy the stability criteria, an aspect ratio of more than 2.80 [11,12, 18] is assumed for all specimens. The isolator denoted by STRP-4/1 in Table 1 is considered for material modelling and model verification.

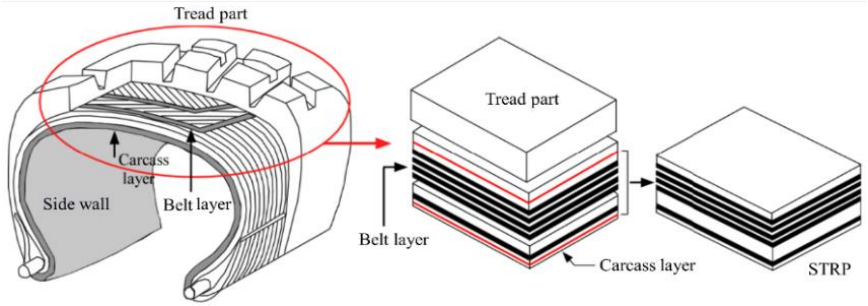

Figure 1 Schematics representation of STRP specimen preparation from scrape tire

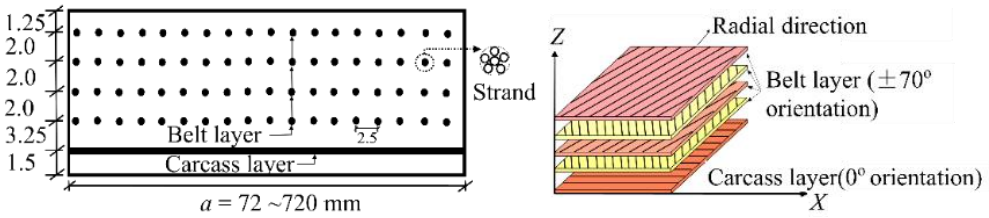

(a) 12-mm Single layer STRP (b) Orientation and number of Reinforcing layer

Figure 2 Reinforcing cords in single layer STRP (Bridgestone tire 385/65R22.5)

Table 1 − Geometric properties of STRP bearing

Bearing Group	Designation	l x w x h (mm)	l/w	t_r (mm)	t_e (mm)	Shape factor, S	Aspect ratio R_l	Aspect ratio R_w
Experiment	STRP-4/1	100x 100 x 48	1	40	2.4	10.4	2.1	2.1
Group-I: Strip	STRP-2/1	72 x 72 x 24	1	20		7.5	3.0	3.0
	STRP-2/2	144 x 72 x 24	2	20	2.4	10	6.0	3.0
	STRP-2/4	288 x 72 x 24	4	20		12	12.0	3.0
	STRP-2/10	720 x 72 x 24	10	20		13.6	*30.0*	3.0

3 Analytical Evaluation of Unbonded STRP Isolator

The horizontal stiffness of a bonded type bearing is given by Eq. (1) in which G is shear modulus and A is the plan area of the isolator [24]. Shear modulus is found to decrease as the lateral strain increases [28, 29] and in case of unbonded type bearings, a significant reduction of the shear modulus occurs within intermediate strain levels [14, 30] followed by a rise after full rollover. In order to express such strain dependence of the shear modulus, the effective modulus, $G_{\text{eff}}^{\text{ub}}$ was proposed by Gerhaher [31, 32] as given by Eq. (2) and Eq. (3). Here, p is vertical pressure on the isolator, u is lateral displacement, a is the isolator dimension parallel to the lateral load, and t_r is the total rubber thickness. $P_{\text{crit},0}$ is called as the critical load capacity of the bearing at zero lateral strain and is given by Eq. (4), where r is the radius of gyration and S is the shape factor [33]. In case of unbonded application, both friction force and friction area changes with lateral deformation and these effects are included in the effective bearing area that remains in contact with supports denoted by A_{eff} defined by Eq. (5) in which d is the projected length of the rollover region, h is the height of the isolator, and γ is a geometric parameter as defined by Eq. (6). The previous study [15] ignored the axial load that causes a reduction of lateral displacement by d_0, which is defined as the displacement corresponding to the initiation of the bearing's separation from the support faces [34, 35]. In the current study, both rollover deformation and axial load are considered using a modified effective area, A_{effm} given by Eq. (7). The stiffness, K_h and equivalent damping ratio β are evaluated using Eq. (8) [36] in which, F^+ and F^- are the positive and negative forces, at the maximum and minimum displacements u^+ and u^-, respectively, and E_{loop} is the area of the force-displacement curve obtained by FE analysis.

$$K_b = \frac{GA}{t_r} \tag{1}$$

$$G_{eff}^{ub} = G\left[1-\left(\frac{p}{p_{\text{crit},0}\left(1-\left(\frac{u}{a}\right)^2\right)}\right)^2\right]\left(1-\frac{u}{a}\right) \quad \text{for } 0 \le u \le t_r \tag{2}$$

$$G_{eff}^{ub} = G\left[1-\left(\frac{p}{p_{\text{crit},0}\left(1-\left(\frac{1.0\,t_r}{a}\right)^2\right)}\right)^2\right]\left(1-\frac{1.0\,t_r}{a}\right) \quad \text{for } 1.0\,t_r < u \le 1.5\,t_r \tag{3}$$

$$p_{\text{crit},0} = \frac{p_{\text{crit}}}{a^2} \quad \text{and} \quad p_{\text{crit}} = \frac{\sqrt{2}\pi GASr}{t_r} \quad \text{where } r = \frac{a}{2\sqrt{3}} \tag{4}$$

$$A_{eff} = b(a-d) \quad \text{where } d = \frac{25}{16}\gamma h \tag{5}$$

$$u = s = \frac{25}{64}h\left[2\gamma\sqrt{1+4\gamma^2} + ln\left(2\gamma+\sqrt{1+4\gamma^2}\right)\right] \tag{6}$$

$$A_{\text{effm}} = b\{a-(d-d_0)\} \quad \text{where} \quad d_0 = H\sqrt{1-\left(1-\frac{p}{E_c}\right)^2} \tag{7}$$

$$K_h = \frac{|F^+|-|F^-|}{|u^+|-|u^-|} \quad \text{and} \quad \beta = \frac{2}{\pi}\left[\frac{E_{\text{loop}}}{K_h\,(|u^+|+|u^-|)^2}\right] \tag{8}$$

4 Finite Element Modelling

4.1 Material Modelling

Tables 2 and 3 describe the properties of reinforcing chords and elastomers of scrap tire obtained from Bridgestone 385/65R22.5. The reinforcing cords are formed by twisted filaments with a yield strength of around 2800 MPa. A hyperelastic behavior of the rubber materials is derived using 3-term using Mooney-Rivlin energy function as given by Eq. (9). Here C_{10}, C_{01}, and C_{11} are material constants, I_1 and I_2 are the first

and second invariants of the Green deformation tensor. The material constants for Bridgestone 385/65R22.5 are shown in Table 3 [22]. Viscoelasticity of rubber is derived as Prony series viscoelastic shear response parameters using a large strain viscoelasticity model [37] as given in Eq. (10) and Eq. (11). Here $W(E_{ij})$ is the standard Mooney-Rivlin strain energy function and $R(t)$ is the relaxation function in the Prony series form, δ^n is a time-dependent scalar multiplier and λ^n the is relaxation time. Elastomer softening is derived from the discontinuous phenomenological damage model representing the so-called Mullin effect through Eq. (12) and Eq. (13), where r and m indicate the damage parameters. Both viscoelastic parameters (δ^n, λ^n) and damage parameters (η, m) parameters are determined through several iterations of FE analysis based on the Mooney-Rivlin material constant. In each iteration, a pair of multiplier and relaxation time parameters are assumed, and then FE analysis is carried out until the hysteresis loop from the experiment is matched with the FE analysis. The best-suited parameters are shown in Table 3.

$$W=C_{10}(I_1-3)+C_{01}(I_2-3)+C_{11}(I_1-3)(I_2-3) \quad (9)$$

$$W(E_{ij}, t) = W(E_{ij})*R(t) \quad (10)$$

$$R(t)=1-\sum_{n=1}^{N}\delta^n(1-exp(-t/\lambda^n)) \quad (11)$$

Unloading case: $$W\frac{\partial\eta}{\partial W}+\eta = 1-\frac{1}{r_1}\tanh[\frac{1}{m_1}(1-\frac{W}{W_m})] \quad (12)$$

Reloading case: $$W\frac{\partial\eta}{\partial W}+\eta = 1-\frac{1}{r_2}\tanh[\frac{1}{m_2}(1-\frac{W}{W_m})] \quad (13)$$

4.2 Modelling of STRP Isolator

The FE analysis is carried out by MSC Marc-Mentat 2018.1.0 [38]. Elastomers are modelled by an isoperimetric hexahedron element best suited for incompressible material with full Herrmann formulation. The reinforcing cords embedded in rubber composite are represented by a hollow and isoperimetric rebar element. Figs. 3a and 3b show the FE models of STRP-4/1 and STRP-2/4, respectively. Superstructure and substructure are modelled as rigid surfaces as shown in Fig. 3. All degrees of freedom of the bottom surface and rotational degrees of freedom of the top surface is constrained. Axial force and lateral displacement are applied at the top surface, as shown in Fig. 3c. The bilinear Coulomb friction model with a friction coefficient 0.80 is used on

Table 2 – Properties of reinforcing cord

Layer	Layer Nos.	Nos. of Filaments	Filament dia (mm)	Single cord area (mm^2)	Orientation	Equivalent thickness t_f(mm)	Yield Strength (MPa)	Spacing (mm)	E (GPa)	v
Carcass	1	5	0.2	0.44	0°	0.40	2800	2.5	200	0.3
Belt	4	14	0.4	0.63	∓72°					

Table 3 – Properties of scrape tire

Mooney-Rivlin Constant			Shear Modulus (MPa)			Prony Shear Responses				Mullin-Damage Parameters			
C_{10}	C_{01}	C_{11}	G_{eff}	G_0	v	δ^1	λ^1	δ^2	λ^2	η_1	m_1	η_2	m_2
0.40	1.22315	0.18759	1.10	1.31	0.49995	0.30	0.2	0.30	0.55	0.01	5	0.05	10

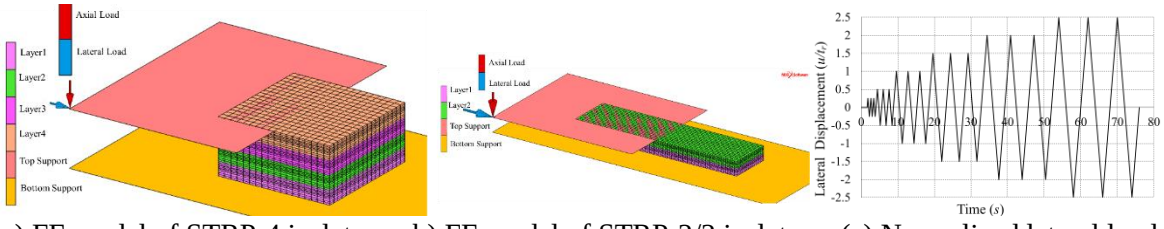

a) FE model of STRP-4 isolator b) FE model of STRP-2/2 isolator (c) Normalized lateral load

Figure 3 Boundary conditions, FE model and loading

contact surface between the rubber layer and the rigid surface as touch contact. In touching contact, each rubber node is constrained along the direction normal to the contact surface and detaching of the rubber node from the contact surface is allowed. The so-called mixed-method proposed by Herrmann is used to derive the stiffness equations. Based on Herrmann's formulation, large strain analysis is used, and kinematics of deformation is solved by Update Lagrangian formulation.

5 FE Model Verification

Table 4 shows the comparison of stiffness values of STRP-4/1 found from the past test results at four magnitudes of lateral strain with the result of FE analysis and proposed evaluation method. A good agreement can be seen among these stiffness values. At large displacements, the proposed evaluation fails to capture the stiffness hardening resulting in a stiffness value around 15% lower than the experimental result. The hysteresis curve shown in Fig. 4a ensured the accuracy of the FE model with the test result and in both cases, the average stiffness found from the slope of hysteresis curves is about 124.5 kN/m. The effective damping obtained by FE analysis is about 16.9% higher than the experimental value. Because of the lack of experimental results for STRP-2/1, the ratios of stiffness and that of damping between experimental results and FE analysis results are used for verification in addition to the analytical solution. The hysteresis loop of STRP-2/1 obtained by FE analysis is shown in Fig. 4b. Table 4 indicates that the results of FE analysis and the proposed evaluation of STRP-2/1 are well agreed. In addition, the ratios of stiffness and damping showed in columns 7 and 10 for STRP-4/1 and STRP-2/1 are varied by 5% only. Therefore, the FE model of STRPs can be regarded as consistent and congruous with the test result.

Table 4 − Horizontal stiffness and damping: Experimental, FEA and Analytical solution

Bearing	u (%t_r)	Horizontal Stiffness, K_h (kN/m)					Effective Damping		
		Experiment	FEA	Analytical	Exp/FEA	FEA/Ana	Experiment	FEA	Exp/FEA
STRP-4/1	37.5	262	258	263.7	1.02	0.98	13.2	15.3	0.86
	75	206	190	188.0	1.08	1.01	12.2	16.5	0.74
	112.5	163	163	138.0	1.00	1.18	14.2	15.8	0.90
	150	133	137	120.0	0.97	1.14	15.0	16.4	0.91
STRP-2/1	37.5	---	298	294.4	----	1.01	13.2	15.5	0.85
	75	---	229	236.3	---	0.97	12.2	16.4	0.76
	112.5	---	201	196.3	---	1.02	14.2	15.2	0.93
	150	---	194	179.8	---	1.08	15.0	14.2	1.06

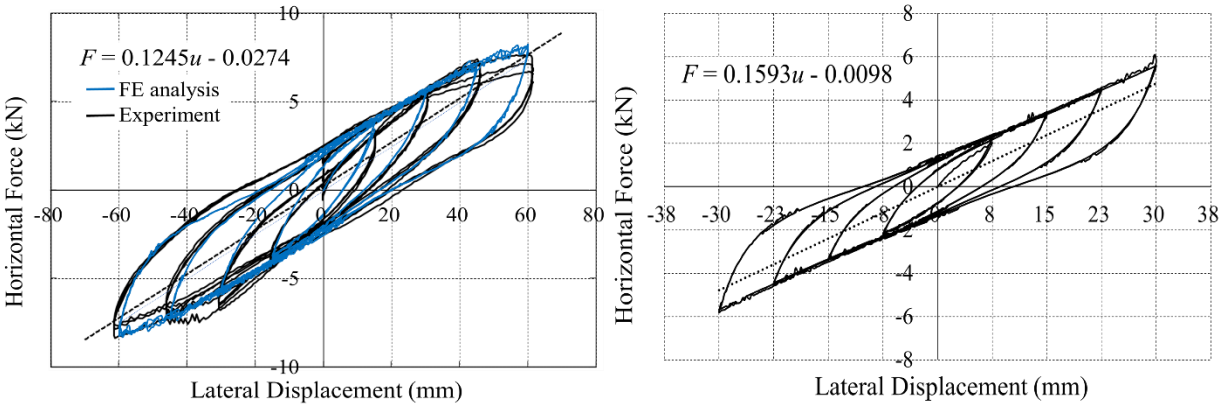

(a) Load-displacement curve of STRP-4/1 (b) Load-displacement curve of STRP-2/1

Figure 4 Hysteresis curve obtained by FE analysis

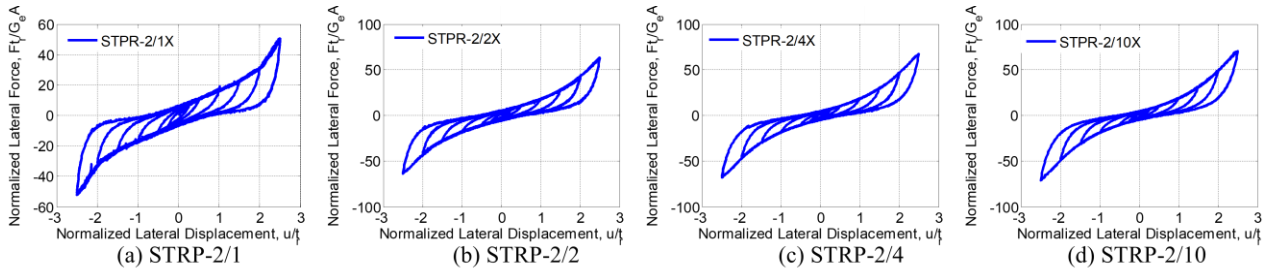

(a) STRP-2/1 (b) STRP-2/2 (c) STRP-2/4 (d) STRP-2/10

Figure 5 Hysteresis curve for longitudinal loading

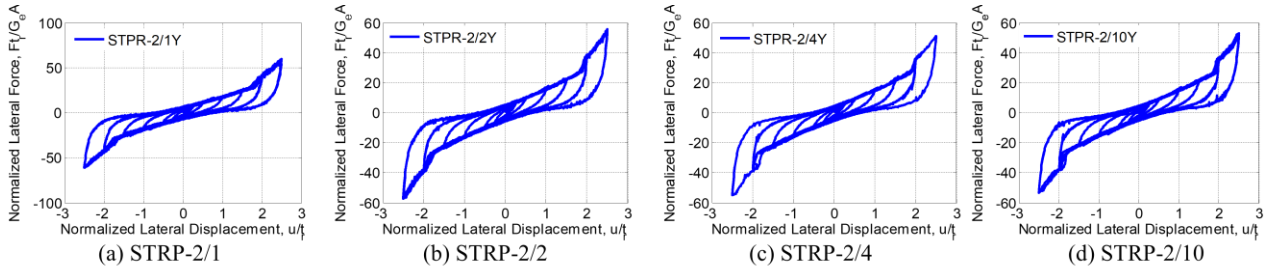

(a) STRP-2/1 (b) STRP-2/2 (c) STRP-2/4 (d) STRP-2/10

Figure 6 Hysteresis curve for transverse loading

6 Lateral Response of Strip-STRP Isolator

6.1 Load-Displacement Relationships

Figs. 5 and 6 show the normalized force-displacement curves of the STRP-2/1, 2/2, 2/4 and 2/10 strip-isolators. In the plots, restoring forces are normalized with $G_{eff}A/t_r$. These hysteresis curves indicate that all isolators exhibit a stable rollover behavior and suffer no slippage until lateral displacement reaches $2.50t_r$. Therefore, the aspect ratio of 3.0 recommended in AASHTO-LRFD method A [27] for bonded type isolators can be also used for the unbonded type as a stability requirement. A high l/w ratio induces the onset of the stiffness hardening at a lower strain level and subsequent quick increase of the restoring force. For example, in the longitudinal direction, the hardening initiates from a displacement such that $u/t_r \geq 1.0$, whereas in the transverse direction it starts from a displacement such that $u/t_r \geq 1.50$. The corresponding normalized restoring forces increase from 20 to 70 in the longitudinal direction. The hysteresis curves of isolator STRP-2/1 indicate that restoring force contribution of the rollover parts is increased for bearing with a low aspect ratio and are negligible for aspect ratios greater than 5.0.

6.2 Horizontal Stiffness and Equivalent Damping Ratio

Figure 7 shows the plots of normalized bearing stiffness ($K_h t_r/G_{eff}A$) at different strain levels for four l/w ratios; The stiffness and damping ratio obtained by the analysis is shown in Tables 5 and 6. The stiffness reduces until the displacement reaches $1.50t_r$ and $1.0t_r$ in the transverse and longitudinal directions, respectively. On the

Table 5 Horizontal stiffness and damping of STRP-2 isolator under longitudinal (X) loading

Normalized displacement (u/t_r)	STRP-2/1		STRP-2/2		STRP-2/4		STRP-2/10	
	K_h (kN/m)	Damping β (%)	K_h (kN/m)	Damping β (%)	K_h (kN/m)	Damping β (%)	K_h (kN/m)	Damping β (%)
$0.25t_r$	339.2	14.31	658.6	12.04	1296.4	11.76	3229.3	11.7
$0.5t_r$	269.3	16.63	528.6	14.59	1071.4	13.69	2699.3	13.5
$1.0t_r$	221.1	15.45	461.8	12.91	970.0	11.93	2500.7	11.6
$1.5t_r$	198.0	14.66	477.3	11.04	1045.4	9.95	2720.8	9.6
$2.0t_r$	201.7	13.39	549.6	9.50	1211.6	8.74	3182.5	8.4
$2.5t_r$	267.3	11.00	657.6	8.85	1404.0	8.40	3670.7	8.2

Table 6 Horizontal stiffness and damping of STRP-2 isolator under transverse (Y) loading

Normalized displacement (u/t_r)	STRP-2/1		STRP-2/2		STRP-2/4		STRP-2/10	
	K_h (kN/m)	Damping β (%)	K_h (kN/m)	Damping β (%)	K_h (kN/m)	Damping β (%)	K_h (kN/m)	Damping β (%)
$0.25t_r$	350.9	12.95	630.1	12.44	1203.0	10.97	2928.3	12.3
$0.5t_r$	274.2	16.10	493.5	15.11	949.5	14.63	2345.0	14.4
$1.0t_r$	222.1	15.09	406.1	14.13	794.5	13.48	1970.8	13.2
$1.5t_r$	205.9	13.85	386.7	12.74	759.6	12.26	1867.4	12.1
$2.0t_r$	268.0	10.66	490.4	9.89	941.5	9.76	2371.5	9.5
$2.5t_r$	314.2	10.77	586.2	9.88	1101.3	10.08	2755.8	9.8

other hand, stiffness increases for displacement greater than those values due to progressive contact and strain hardening. In general, normalized stiffness of STRP exhibits the minimum value in the range of 0.7~1.0 within the strain range $1.0t_r$~$1.50t_r$ which can be considered as a basis for DBE design. Stiffness fluctuation between intermediate ($1.0t_r$~$1.5t_r$) and large strain levels ($2.50t_r$) becomes more significant for low aspect ratio cases. As the *l/w* ratio increases, the longitudinal stiffness increases whereas the transverse stiffness shows a minor decrease. For example, longitudinal stiffness increased by 37.4%, 57.8% and 37.5% at displacement $1.5t_r$, $2.0t_r$ and $2.5t_r$ respectively, for *l/w* ratio increase to 10 from 1. Conversely, the transverse stiffness decreased on average by 12% only at each level of lateral displacement. Therefore, a higher l/w ratio can diminish the efficiency of the isolation system.

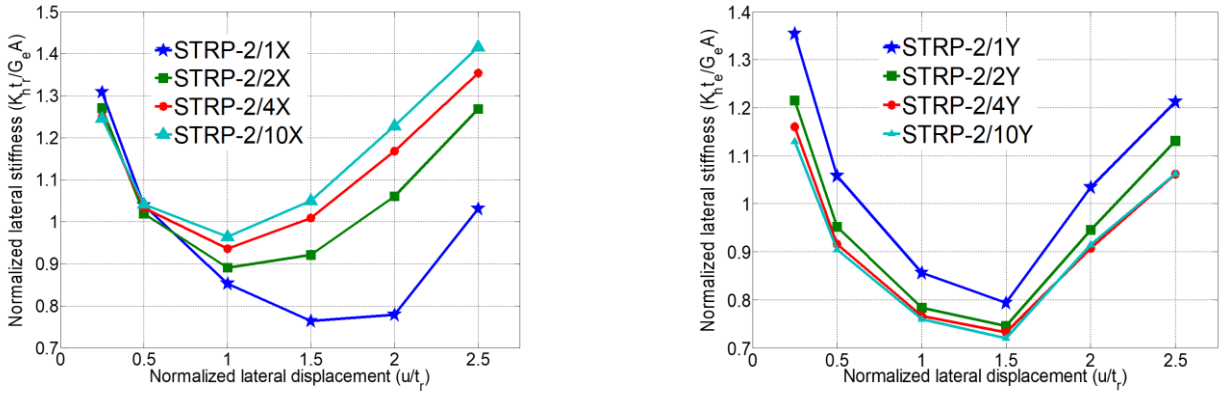

(a) Longitudinal direction (b) Transverse direction

Figure 7 Relationship between horizontal stiffness and lateral displacement

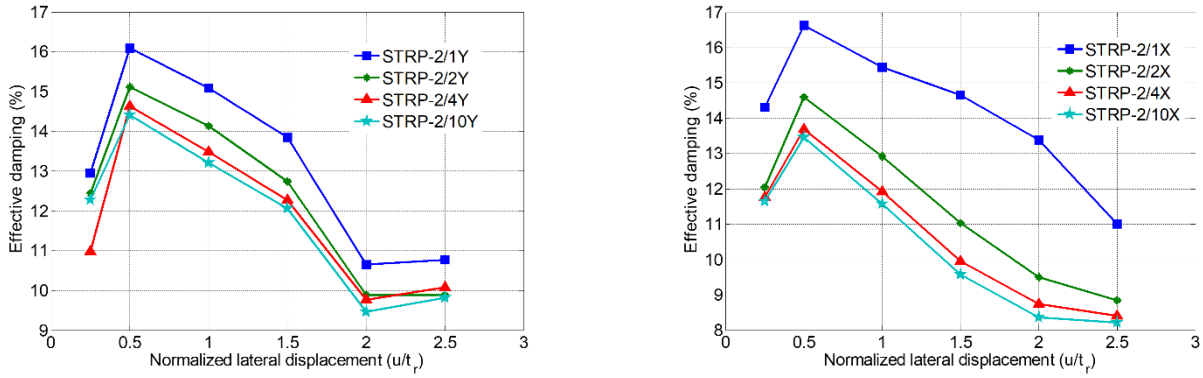

(a) Longitudinal direction (b) Transverse direction

Figure 8 Relationship between equivalent damping and lateral displacement

Figure 8 shows the relationship between the equivalent damping ratio and the bearing displacement. The effective damping ratio tends to be lower for a high value of *l/w* ratio and for a displacement larger than $0.5t_r$. The *l/w* ratio as high as 10 causes an average damping reduction of about 26.5% and 10.3% in the longitudinal and transverse directions, respectively. At the displacement of $2.5t_r$, the effective damping ratio decreased by 38% and 33% for the longitudinal and transverse directions, respectively. Based on these results, the minimum damping of STRP for the DBE level in the displacement range of $1.0t_r$ ~$1.50\ t_r$ can exceed 10%.

7 Seismic Performance Evaluation

The seismic performance of strip STRP isolators is assessed for two earthquake levels: DBE and MCE. The maximum design lateral displacement (D_D) and effective period (T_D) of an STRP isolator are determined by Eq. (14), where g is the gravitational acceleration (mm/s^2); S_{D1} is 5% damped DBE spectral acceleration at period of 1s and is given by Eq.(15); T_D is the isolation period (*s*); W is the effective seismic weight (5.0 MPa), k_{hmin} is the minimum effective stiffness (kN/mm), B_D is the damping coefficient, S_1 is risk-targeted MCE spectral acceleration for a period of 1s, and F_v is the site class coefficient obtained from ASCE-2010: Table 11.4-2. For MCE level, displacement, D_M and period, T_M are obtained by substituting the suffix D by M.

$$D_D = \frac{gS_{D1}\,T_D}{4\pi^2 B_D} \quad \text{and} \quad T_D = 2\pi\sqrt{\frac{W}{k_{hmin}\,g}} \tag{14}$$

$$S_{M1} = F_v\,S_1 \quad \text{and} \quad S_{D1} = 2/3\ S_{M1} \tag{15}$$

Both the displacement and the period are calculated with an iterative procedure [10]. First, for a fixed value of S_1 and specific site class, coefficient F_v and then S_{M1} and S_{D1} are calculated. The allowable displacement limits of STRP at DBE and MCE levels are assumed in the range of $1.0t_r$ ~ $1.50t_r$ and $2.0t_r$ ~ $2.50t_r$, respectively, and the corresponding equivalent damping ratio and the damping coefficient, B_D and B_m are given in Tables 7 and 8. Each iteration is started with an initial value of $D_D = 1.0t_r$ and the corresponding stiffness, K_{hmin} is taken from Table 5 or 6 to obtain the period T_D. Then the period of the full-scale isolator is calculated by the similitude law. The displacement demand for the full-scale isolator, D_D is then determined by Eq. (19). In the second step, the stiffness of the reduced scale isolator is updated from Table 5 or 6 based on the updated demand displacement, D_D and then the period, T_D and displacement, D_D are subsequently calculated. This procedure is continued until the values of T_D or D_D converge with a sufficiently small error tolerance. A similar iterative procedure is used for the period, T_M and displacement, D_M at the MCE level.

7.1 Performance of Strip-STRP isolator

Table 7 shows the displacement demand and isolation period of 96 mm high STRP isolator at class C site such that S_1=0.40. The corresponding spectral accelerations for DBE and MCE are 0.373g and 0.56g, respectively. In the longitudinal direction, the isolation periods at DBE and MCE ($T_D \approx$ 1.27~1.42s and $T_M \approx$ 1.18~1.40s) are substantially longer than the limit value of 1.0 s at which an earthquake contains maximum energy [39] and corresponding displacement demand ($D_D \approx 1.17t_r$~$1.31t_r$ and $D_M \approx 1.78t_r$~$2.09t_r$) do not exceed the allowable limit. In the transverse direction, the periods and displacement demands are larger than that of longitudinal direction by 20% and 15%, respectively.

Similarly, Table 8 describes the bearing performance at class D site such that S_1 = 0.50. The spectral accelerations for DBE and MCE in this case are 0.5g and 0.75g, respectively. In the longitudinal direction, the isolation periods of the bearings are longer than 1.0 s ($T_D \approx$ 1.23~1.44 s and $T_M \approx$1.11~1.25 s) and the displacement demand at DBE level, $D_D \approx 1.52t_r \sim 1.83t_r$ exceeds the allowable displacement limit ($1.5t_r$). The displacement demand at MCE level, $D_M \approx 2.22t_r$ ~$2.51t_r$ almost satisfies the upper limit requirement ($2.50t_r$). In the transverse direction, both the period and displacement demand of the isolators are about 15% larger than that of the longitudinal direction. In both directions, the period at MCE level is shorter than the period at DBE level because of stiffness hardening, and the bearing displacement demand at MCE level is found to be lower than the capacity requirement for MCE. In all cases, the periods are longer than 1.11s, implying that a 96 mm bearing can satisfactorily be used for the above-mentioned site conditions.

Table 7 − Performance of full scale bearing at a class C sit of S_1=0.40

1/4th scale model	Full scale model (mm)	Damping β		Damping Coefficient		Spectral Acceleration		Isolation Periods (s)		Max. Shear strain	
		DBE	MCE	B_D	B_M	S_{D1}	S_{M1}	DBE	MCE	DBE	MCE
Longitudinal direction											
STRP-2/1	STRP-8/1: 288x288x96	12%	9%	1.26	1.16	0.373g	0.56g	1.42	1.40	1.31	2.09
STRP-2/2	STRP-8/2: 576x288x96							1.33	1.25	1.23	1.88
STRP-2/4	STRP-8/4:1152x288x96							1.29	1.21	1.19	1.81
STRP-2/10	STRP-8/10: 2880x288x96							1.27	1.18	1.17	1.78
Transverse direction											
STRP-2/1	STRP-8/1: 288x288x96	13%	10%	1.29	1.20	0.373g	0.56g	1.42	1.22	1.25	1.86
STRP-2/2	STRP-8/2: 576x288x96							1.47	1.26	1.31	1.92
STRP-2/4	STRP-8/4:1152x288x96							1.48	1.28	1.32	1.95
STRP-2/10	STRP-8/10: 2880x288x96							1.50	1.28	1.33	1.95

Table 8 Performance of full scale bearing at class D site of S_1=0.50

1/4thscale model	Full scale model	Damping β		Damping Coefficient		Spectral Acceleration		Isolation Periods (s)		Max. Shear strain	
		DBE	MCE	B_D	B_M	S_{D1}	S_M1	DBE	MCE	DBE	MCE
Longitudinal direction											
STRP-2/1	STRP-8/1:288x288x96	12%	9%	1.26	1.16	0.5g	0.75g	1.44	1.25	1.83	2.51
STRP-2/2	STRP-8/2:576x288x96							1.30	1.16	1.60	2.33
STRP-2/4	STRP-8/4:1152x288x96							1.25	1.13	1.54	2.26
STRP-2/10	STRP-8/10:2880x288x96							1.23	1.11	1.52	2.22
Transverse direction											
STRP-2/1	STRP-8/1:288x288x96	13%	10%	1.29	1.20	0.5g	0.75g	1.37	1.26	1.64	2.45
STRP-2/2	STRP-8/2:576x288x96							1.40	1.22	1.69	2.37
STRP-2/4	STRP-8/4:1152x288x96							1.41	1.25	1.70	2.42
STRP-2/10	STRP-8/10:2880x288x96							1.42	1.24	1.71	2.42

Conclusion

3-D FE analysis is carried out to investigate the lateral performance of the strip STRP isolator. From the findings of the FE analysis, the following conclusions can be drawn:

- The minimum stiffness of the strip STRP isolator is in the range of 0.70~1.0 times of that based on the effective shear modulus, and the minimum equivalent damping ratio is 10% within the strain range of 1.0~1.5. These are the expected performance of strip-shaped STRP isolators DBE level design.
- Dependence of stiffness on the length-width ratio *l/w* is significant in the longitudinal direction and minor in the transverse direction. Stiffness is increased by 37~58% in the longitudinal direction while it is decreased by 12% in the transverse as *l/w* increases from 1 to 10.
- At a large displacement of $2.50t_r$, the equivalent damping ratio of the strip STRP isolator decreases by 38% and 33% in the longitudinal and transverse directions, respectively. Dependence of damping on *l/w* is insignificant for a value larger than 4.0.
- For both class C site spectrum of S_1=0.40 and class D site spectrum of S_1=0.50, the isolated period with the strip STRP isolator is found to be longer than 1.11 s, and the period at MCE level is shorter than that of DBE level. The displacement demand of a 96 mm STRP isolator is found to be lower than the capacity requirement for MCE. At class D site of S1=0.50, bearing capacity exceeds the displacement demand at the DBE level, whereas the stiffness hardening limits the bearing displacement below than the tolerable value at MCE level. The displacement demand and the period of STRP in the transverse direction are about 15% and 20% higher than that in the longitudinal direction.

Since the lateral performance of STRP is evaluated through FE analysis and an iterative method based on the experimental and interpolating properties of elastomer, experimental verification of the proposed recommendations is needed for a concrete conclusion on seismic performance of strip-STRP isolators.

References

[1] Kelly JM (2002): Seismic isolation systems for developing countries. *EERI Distinguished Lecture*, Earthquake Spectra, 18(3), 385–406.

[2] Pan P, Zamfirescu D, Nakashima N, Nakayasu N and Kashiwa H (2005): Base–isolation design practice in Japan: Introduction to the post–Kobe approach. *J. Earthquake Engineering*, 9(1), 147–171.

[3] May PJ (2002): Barriers to adoption and implementation of PBEE innovations. *PEER Rep. 2002/20*, Pacific Earthquake Engineering Research Center, University of California, Berkeley.

[4] Kelly MJ and Takhirov SM (2001): Analytical and experimental study of fiber reinforced strip isolators. *PEER report 2002/11*, Dept. of Civil and Environmental Engineering, University of California, Berkeley.

[5] De la Llera JC, Lüders C, Leigh P and Sady H (2004): Analysis, testing, and implementation of seismic isolation of buildings in Chile. *Earthquake Engineering and Structural Dynamics*, 33(5), 543–574.

[6] Turer A and Özden B (2007): Seismic base isolation using low-cost scrap tire pads (STP). *Materials and Structures*, 41(5), 891-908.

[7] Xiao H, Butterworth JW and Larkin T (2004): Low-technology techniques for seismic isolation. *New Zealand Society of Earthquake Engineering Conference*, paper No. 36

[8] Tsang H-H (2008). Seismic isolation by rubber-soil mixtures for developing countries. *Earthquake Engineering and Structural Dynamics*, 37 (2), 283-303.

[9] Kelly JM (1999): Analysis of fiber-reinforced elastomeric isolators. *J. of Seismology and Earthquake Engineering*, 2(1), 19–34.

[10] Toopchi-Nezhad H, Tait MJ, Drysdale RG (2008a): Lateral Response Evaluation of Fiber-Reinforced Neoprene Seismic Isolators Utilized in an Unbonded Application. *J. of Structural Engineering*, 134(10), 1627–1637.

[11] Toopchi-Nezhad H, Tait MJ and Drysdale RG (2008b): Testing and modeling of square fiber-reinforced elastomeric seismic isolators. *Structural Control Health Monitoring*, 15(6), 876-900.

[12] Toopchi-Nezhad H, Drysdale RG and Tait MJ (2009a): Parametric Study on the Response of Stable Unbonded-Fiber Reinforced Elastomeric Isolators (SU-FREIs). *J. of Composite Materials*, 43(15), 1569-1587.

[13] Toopchi-Nezhad H, Tait MJ and Drysdale RG (2009b): Shake table study on an ordinary low-rise building seismically isolated with SU-FREIs (stable unbonded-fiber reinforced elastomeric isolators). *Earthquake Engineering and Structural Dynamics*, 38(11), 1335-1357.

[14] Toopchi-Nezhad H, Tait MJ, Drysdale RG (2011): Bonded versus unbonded strip fiber reinforced elastomeric isolators finite element analysis. *Composite Structures*, 93(2), 850–859.

[15] Toopchi-Nezhad H (2014): Horizontal stiffness solutions for unbonded fiber reinforced elastomeric bearings. *Structural Engineering and Mechanics*, 49(3), 395–410.

[16] Al-Anany YM and Tait MJ (2015): A numerical study on the compressive and rotational behavior of fiber reinforced elastomeric isolators (FREI). *Composite Structures*, 133, 1249-1266.

[17] Al-Anany YM, Van Engelen NC and Tait MJ (2017): Vertical and Lateral Behavior of Unbonded Fiber-Reinforced Elastomeric Isolators. *J. of Composite for Construction*, 21(5), 1-11.

[18] Van Engelen, N. C., Tait, M. J., and Konstantinidis, D., (2015): "Model of the shear behavior of unbondedfiber-reinforced elastomeric isolators." J. Struct. Eng., ASCE, 141 (7), 1-11.

[19] Spizzuoco M, Calabrese A and Serino G (2014): Innovative low-cost recycled rubber-fiber reinforced isolator: Experimental tests and Finite Element Analyses. *Engineering Structure*, 76(1), 99-111.

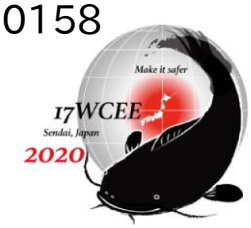

[20] Calabesre A, Spizzuoco M, Serino G, Corte GD and Maddaloni G (2015): Shaking table investigation of a novel, low-cost, base isolation technology using recycled rubber. *Structural Control Health Monitoring*, 22(1), 107-122.

[21] Mishra HK (2012): Experimental and Analytical Studies on Scrap Tire Rubber Pads for Application to Seismic Isolation of Structures. *Ph.D. Thesis*, Kyoto University, Japan.

[22] Mishra HK, Igarashi A, Matsushima H (2013a): Finite element analysis and experimental verification of the scrap tire rubber pad isolator. *Bulletin Earthquake Engineering*, 11(2), 687-707.

[23] Mishra HK and Igarashi A (2013b): Lateral deformation capacity and stability of layer-bonded scrap tire rubber pad isolators under combined compressive and shear loading. *Structural Engineering and Mechanics*, 48(4), 479-500.

[24] Kelly JM (1997): *Earthquake-resistant design with rubber*, 2nd Ed., London, Springer-Verlag.

[25] Eurocode 8 (2004): *Design of structures for earthquake resistance*, BS EN 1998-1:2004.

[26] Tsai HC and Kelly JM (2002). Stiffness analysis of fiber-reinforced rectangular seismic isolators. *J. Engineering Mechanics*, 128(4), 462–470.

[27] AASHTO-LRFD (2014): LRFD Bridge Design Specifications, 7th Ed., Washington, D. C.

[28] Ashkezari GD, Aghakouchak AA, Kokabi M (2008): Design, manufacturing and evaluation of the performance of steel like fiber reinforced elastomeric seismic isolators. *Journal of Material Processing Technology*, 197, 140–150.

[29] Strauss A, Apostolidi E, Zimmermann T, Gerhaher U and Dritsos S (2014): Experimental investigations of fiber and steel reinforced elastomeric bearings: shear modulus and damping coefficient. *Engineering Structures*, 75, 402–413

[30] Das A, Dutta A and Deb SK (2014): Performance of fiber-reinforced elastomeric base isolators under cyclic excitation. *Structural Control Health Monitoring*, 22, 197-220.

[31] Gerhaher U, Strauss A and Bergmeister K (2011): Verbesserte Bemessungsrichtlinien für Bewehrte Elastomerlager. *Bautechnik*, 88(7), 451–458 [in German].

[32] Ngo TV, Dutta A, and Deb SK (2017): Evaluation of horizontal stiffness of fibre-reinforced elastomeric isolators. *Earthquake Engineering and Structural Dynamics*, 46, 1747-1767.

[33] Kelly JM (2003): Tension buckling multilayer elastomeric bearings. *Journal of Engineering Mechanics*, 129 (12), 1363–1368

[34] Russo G, Pauletta M and Cortesia A (2013): A study on experimental shear behavior of fiber-reinforced elastomeric isolators with various fiber layouts, elastomers and aging conditions, *Engineering Structure*, 52, 422 433.

[35] Pauletta M, Cortesia A, and Russo G (2015): Roll-out instability of small size fiber-reinforced elastomeric isolators in unbonded applications. Engineering Structures, 102, 358–368.

[36] ASCE/SEI 7-10 (2010): *Minimum Design Loads for Buildings and Other Structures*, ASCE, 1801 Alexander Bell Drive, Reston, Virginia.

[37] Simo JC (1987): On a Fully Three-dimensional Finite Strain Viscoelastic Damage Model: Formulation and Computational Aspects, *Computer Methods in Applied Mechanics and Engineering*, 60, 153-173.

[38] MSC. Marc-Mentat, *Theory and user information*, Vol. A, Santa Ana, CA: MSC Software Corporation; 2018.

[39] Skinner RI, Robinson WH and McVerry GH (1993): *An introduction to seismic isolation*, Wiley, Chichester, U.K.

